JOURNAL OF MATERIALS SCIENCE 17 (1982) 2801–2808

Prediction of the stress–strain curve of a short-fibre reinforced thermoplastic

MINORU TAYA, TSU-WEI CHOU
Department of Mechanical and Aeorospace Engineering, University of Delaware, Newark, Delaware 19711, USA

Analytical work has been performed to predict the stress–strain curve of a carbon fibre reinforced polyamide 66. A typical stress–strain curve of this composite consists of three stages. Beyond the first linear stage the change of slope of the curve is attributed to the initiation and extension of cracks at fibre ends. Several theoretical models have been developed to take into account the development of cracks at various loading levels. Fibre volume-fraction, aspect ratio and orientation as well as fibre and matrix elastic properties and interface energies are the major parameters considered. The theoretical predictions are in close agreement with the experimental data.

1. Introduction

Short-fibre reinforced resins and metals have emerged as composites of major technological significance in recent years. The thermomechanical behaviour of short-fibre composites has been given considerable attention by researchers regarding their stiffness [1], thermal conductivity [2], thermal expansion [3] and strength [4]. This paper is devoted to the study of the load–deformation behaviour of short-fibre composites with particular attention on reinforced thermoplastics.

A typical stress–strain curve of short-fibre reinforced thermoplastics has basically three stages [5], the first stage being linear, and the second and third stages being non-linear as shown in Fig. 1 for the case of graphite short-fibre (10% volume-fraction) reinforced nylon. It has been observed that in the first stage the bonding of the matrix–fibre interface is essentially perfect and both phases deform elastically, and in the second stage microcracks are initiated from fibre ends and they extend into the matrix. In the third stage the microcracks are abundant and some of them grow to a large size, leading to the failure of the composite. The non-linearity in the second and third stages is due to the initiation and development of microcracks.

Taya and Chou [6] have simulated the stress–strain curve of unidirectional short-fibre reinforced thermoplastics, and have solved the following problems:

(1) Prediction of the longitudinal Young's modulus of the first stage, $E_L^{(1)}$.

(2) Prediction of the transition stresses σ_1 between the first and second stages, and σ_2 between the second and third stages.

(3) Prediction of the longitudinal Young's modulus of the second stage weakened by the microcracks, $E_L^{(2)}$.

In this paper the focus is on misoriented short-fibre composites which is the case given in [5]. To this end, two analytical methods developed by the authors will be employed. The first method [7] is for computing the stiffness of randomly oriented short-fibre composites, and the second [8] is for predicting the critical applied stress at which a penny-shaped crack arrested by the adjacent fibres penetrates the arresting fibres. In this paper we will also employ a refined model for evaluating cumulative crack density function.

The analytical techniques used in this study, as well as our previous works, are mainly based on Eshelby's equivalent inclusion method [9] and the solution procedure based upon this method has been discussed elsewhere, for example, [10, 11]. Thus we will discuss only briefly the solution procedure to compute $E_L^{(1)}$ in Section 2, σ_1 in Section 3, σ_2 in Section 4, and $E_L^{(2)}$ in Section 5.

0022–2461/82/102801–08$03.46/0

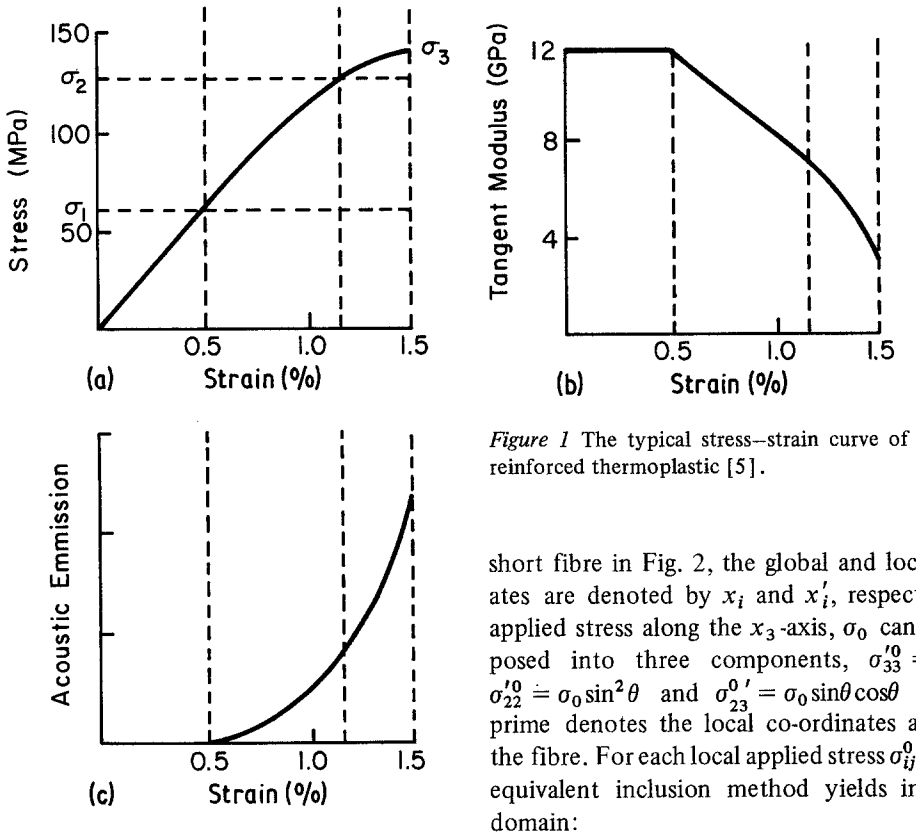

Figure 1 The typical stress–strain curve of a short-fibre reinforced thermoplastic [5].

Analytical results are obtained for 20% volume fraction of graphite short-fibre composite and they are compared with experimental data in Section 6. Finally, the conclusions are given in Section 7.

2. Prediction of $E_L^{(1)}$

In order to compute the longitudinal Young's modulus of misoriented short-fibre composites in the first stage, $E_L^{(1)}$, the theoretical model shown in Fig. 2 is considered. It is assumed in this model that all short fibres are elongated ellipsoids of the same size and oriented randomly within certain limits and the composite possesses transverse isotropy. The probability density function, $g(\theta)$, is taken as

$$g(\theta) = \begin{cases} \dfrac{1}{\alpha}, & 0 \leqslant \theta \leqslant \alpha \\ 0, & \alpha \leqslant \theta \leqslant \dfrac{\pi}{2} \end{cases} \quad (1)$$

where θ is the orientation angle of a short fibre with respect to the x_3-axis (loading direction) as shown in Fig. 2, and α is the limit of θ.

The analytical method of computing $E_L^{(1)}$ has recently been developed by Takao *et al.* [7] and is reviewed briefly below. Refering to a typical short fibre in Fig. 2, the global and local coordinates are denoted by x_i and x_i', respectively. The applied stress along the x_3-axis, σ_0 can be decomposed into three components, $\sigma_{33}'^0 = \sigma_0 \cos^2\theta$, $\sigma_{22}'^0 = \sigma_0 \sin^2\theta$ and $\sigma_{23}^{0\,\prime} = \sigma_0 \sin\theta\cos\theta$ where the prime denotes the local co-ordinates attached to the fibre. For each local applied stress $\sigma_{ij}^{0\prime}$, Eshelby's equivalent inclusion method yields in the fibre domain:

$$C_{ijkl}^0(\epsilon_{kl}^{0\prime} + \tilde{\epsilon}_{kl}' + \epsilon_{kl}' - \epsilon_{kl}^{*\prime}) = C_{ijkl}^{\mathrm{f}}(\epsilon_{kl}^{0\prime} + \tilde{\epsilon}_{kl}' + \epsilon_{kl}'), \quad (2)$$

where

$$\sigma_{ij}^{0\prime} = C_{ijkl}^0 \epsilon_{kl}^{0\prime}, \quad (3)$$

$$\epsilon_{kl}' = S_{klmn} \epsilon_{mn}^{*\prime} \quad (4)$$

and

$$\langle \sigma_{ij}' \rangle_{\mathrm{M}} = C_{ijkl}^0 \tilde{\epsilon}_{kl}'. \quad (5)$$

In the above equations, $\langle \sigma_{ij}' \rangle_{\mathrm{M}}$ is the average of the stress disturbance in the matrix, σ_{ij}' and ϵ_{ij}' are the disturbances of the stress and strain, respectively, caused by this single fibre, $\epsilon_{kl}^{*\prime}$ is called eigenstrain which assumes some value in the fibre, but vanishes in the matrix, and S_{klmn} is the Eshelby's tensor. C_{ijkl}^0 and C_{ijkl}^{f} denote elastic stiffness constants of the matrix and fibre, respectively. Since the integration of stress disturbance over the entire composition domain vanishes, $\int \sigma_{ij} \mathrm{d}V = 0$ [10–13], gives

$$C_{ijkl}^0 \tilde{\epsilon}_{kl} + \langle \sigma_{ij} \rangle_{\mathrm{F}} = 0. \quad (6)$$

Using Equation 6 and co-ordinate transformation, the eigenstrain in the global co-ordinate, ϵ_{ij}^*, can be solved. E_{L} can then be computed by substitut-

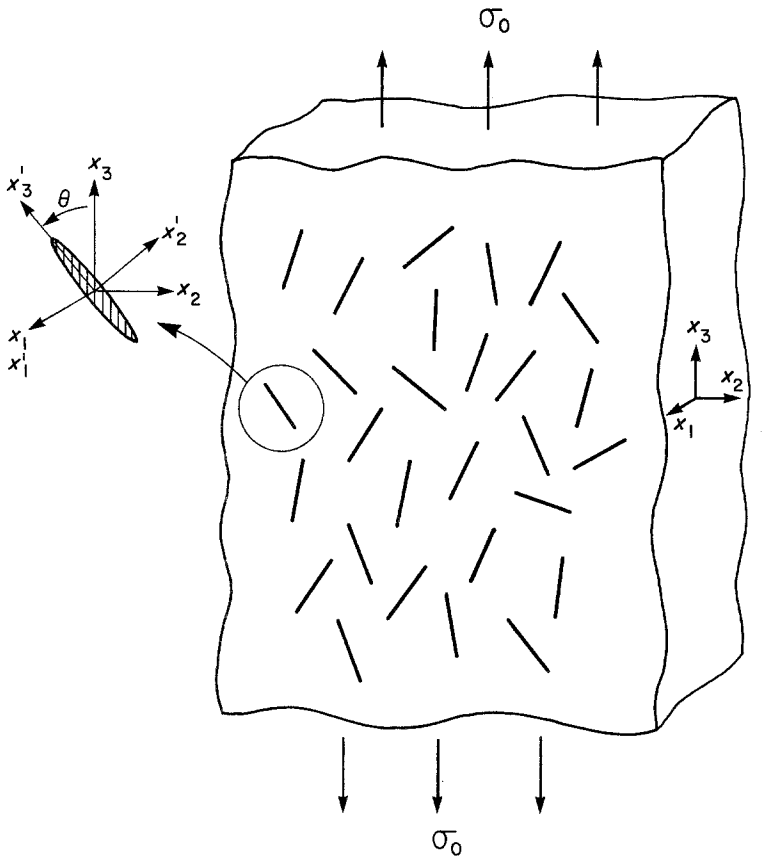

Figure 2 A theoretical model for a randomly oriented short-fibre reinforced composite.

ing ϵ_{ij}^* into the equation of equivalence of strain energy:

$$\frac{\sigma_0^2}{2E_L} = \frac{\sigma_0^2}{2E_m} + \frac{1}{2V_0}\int_{V_F} \sigma_{33}^0 \epsilon_{33}^* \, dV, \qquad (7)$$

Where E_m is Young's modulus of the matrix, V_0 and V_f are, respectively, the volumes of the composite and all fibres. ϵ_{33}^* is a component of the eigenstrain and it is a function of the elastic constants of the matrix and fibre, the aspect ratio of the fibre and θ.

We also introduce an orientation factor in the first stage, g_1, for the convenience of later calculations. g_1 is defined as

$$g_1 = \frac{E_L^{(1)}}{\bar{E}_L^{(1)}}, \qquad (8)$$

where $\bar{E}_L^{(1)}$ is the longitudinal Young's modulus of the composite where all short fibres are aligned in the loading direction, and $E_L^{(1)}$ is that of the misoriented short-fibre composite.

3. Prediction of σ_1

In order to predict the transition stress between the first and second stages, σ_1, it is assumed that under the applied stress σ_1 a penny-shaped crack is initiated from the end of a short fibre which is aligned with the loading direction (Fig. 3) while a majority of the fibres are randomly oriented. In order to account for the random orientation of short fibres, the following steps are adopted:

(a) Compute σ_1 for the case of completely aligned short-fibre system.

(b) Multiply σ_1 obtained above by the orientation factor h_1 which will be defined in Equation 12.

The first step has been performed by Taya and Mura [10], who use two calculation models: the composite before a fibre-end crack is initiated (Fig. 3a) and that after it is initiated (Fig. 3b). The analytical methods of [6] are briefly reviewed below.

Consider the total free energy of the composite before (U_1) and after (U_2) the fibre-end crack is initiated. In order for a small penny-shaped crack to initiate at the fibre-end, the following inequality must be satisfied,

$$U_1 \geqslant U_2. \qquad (9)$$

In [10], the above inequality can be expressed as

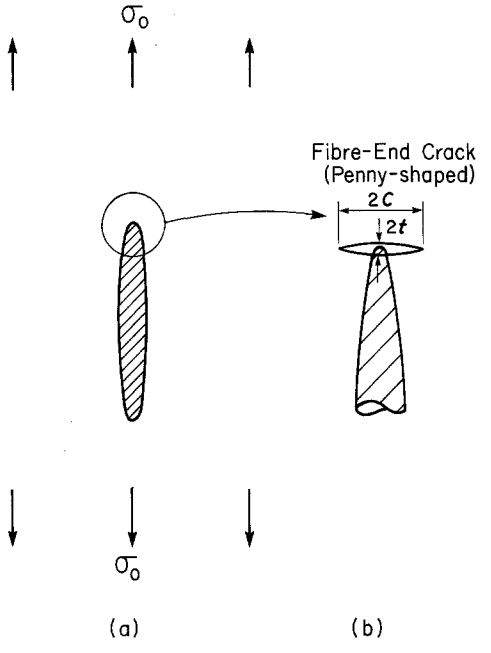

Figure 3 The model for calculating σ_1.

$$\frac{8}{3}\frac{\sigma_0^2(1-\nu_m^2)(1+\xi_1)C^3}{E_m} \geqslant \pi C^2\gamma_m, \qquad (10)$$

where ν_m and γ_m are Poisson's ratio and the surface energy of the matrix, respectively. C is the radius of the penny-shaped crack and ξ_1 is a fibre interaction parameter which is a function of the elastic constants of the matrix and fibre, the fibre aspect ratio and the volume-fraction of fibre f_F. Also in Equation 10 we have assumed that the order of magnitude of the surface energy of the matrix–fibre interface γ_I is much smaller than that of γ_m.*

To account for the random orientation of the short fibres, we assume that the effective applied stress for a short fibre at an angle θ with respect to the x_3-axis (Fig. 2) is $\sigma_0\cos^2\theta$ by neglecting the shear and transverse stress components. By replacing σ_0^2 in Equation 10 with $\sigma_0^2\cos^4\theta$ and considering the contribution of all misaligned fibres, we obtain

$$\sigma_1 = h_1\left(\frac{3\pi\gamma_m E_m}{8(1-\nu_m^2)(1+\xi_1)C}\right)^{1/2}, \qquad (11)$$

where h_1 in Equation 11 is the orientation factor and is defined by

$$h_1 = \int_0^\alpha \cos^4\theta\,\frac{1}{\alpha}\,d\theta. \qquad (12)$$

4. Prediction of σ_2

It is assumed that the end of the second stage corresponds to the moment when the fibre end crack in the position as indicated by the solid curve in Fig. 4 is just about to extend further in the matrix. The critical stress σ_2 for the penny-shaped crack of radius $C_1 + C_2$ (Fig. 4) to propagate as a Griffith-type crack is

$$\sigma_2 = \left(\frac{\pi\gamma_m E_m}{2(1-\nu_m^2)(C_1+C_2)}\right)^{1/2} \qquad (13)$$

We comment here on the extension of the crack arrested by the adjacent fibres from the position indicated by the dotted line to the position shown by the solid line in Fig. 4. Growth of cracks of this type has been examined by Ishikawa *et al.* [8]. They investigated the critical applied stresses necessary for the crack to propagate into the fibre (penetration type) or into the fibre–matrix interface (debonding type). In Section 6.3 it is shown that, for the short fibre composite system studied here, fibre penetration or interfacial debonding occurs at a stress level below that of σ_2. It is thus feasible for the crack to extend into the matrix at

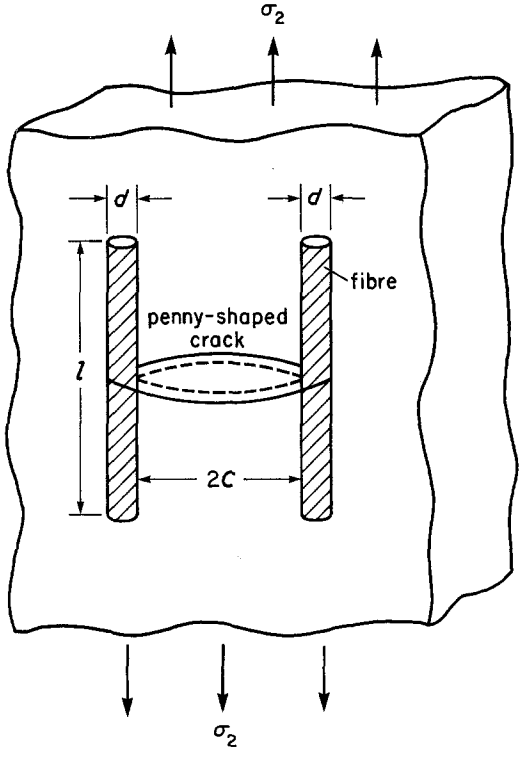

Figure 4 The model for calculating σ_2. The short fibre at which the crack was initiated is not shown.

*If we include the effect of γ_I in computing σ_1, then γ_m in Equation 11 should be replaced by $\gamma_m + \gamma_I$.

the beginning of the third stage of the stress–strain curve.

In Fig. 4, we consider the special configuration where the fibres are in the position of being aligned with the applied load. As far as the extension of the penny-shaped crack, and hence the third stage deformation, are concerned this may be the most probable configuration. For cracks meeting fibres inclined to the crack plane, extensive interface debonding is most likely to occur. Thus the crack will be rendered ineffective, and the third stage deformation may be suppressed.

5. Prediction of $E_L^{(2)}$

In the second stage, the density f_c of penny-shaped cracks in the composite is defined as

$$f_c = \frac{NC^3}{V}, \tag{14}$$

where N is the total number of cracks, C is the radius of penny-shaped cracks, and V is the total volume of the body. It is further assumed that at the end of the second stage all the fibres have initiated penny-shaped crack of radius $C = 1.5d$ [5]. Then the crack density at the end of the second stage, $f_c^* = 0.0516$ for $l/d = 50$. In order to compute $E_L^{(2)}$ at all stress levels between σ_1 and σ_2, we assume that the crack density of the composite is governed by the stress levels as

$$f_c = \alpha_1 \tan\left(\frac{\sigma - \sigma_1}{\sigma_2 - \sigma_1}\right), \tag{15}$$

where $\alpha_1 = 0.1284$ for $f_c^* = 0.0516$. The choice of Equation 15 is made based on the acoustic emission result [5]. For σ between σ_1 and σ_2, some fibres remain intact and the others have developed fibre-end cracks. Thus, the volume-fraction of fibres with no cracks attached f_F, is given by

$$f_F = \alpha_2 \left[\alpha_3 - \tan\left(\frac{\sigma - \sigma_1}{\sigma_2 - \sigma_1}\right)\right], \tag{16}$$

where $\alpha_2 = 0.1284, \alpha_3 = \tan 1$ for $f_c^* = 0.0516$.

Based upon Equations 15 and 16, we proceed to compute $E_L^{(2)}$ at various stress levels. However, an exact calculation of $E_L^{(2)}$ for a randomly oriented short fibre composite with fibre-end cracks is extremely difficult. Hence we compute E_L for the completely aligned case and then multiply it by the orientation factor g_1 defined in Equation 8. A computation of E_L of a completely aligned short-fibre composite where some of the fibres have initiated penny-shaped cracks at their ends has recently been made by Takao *et al.* [14]. The effect of fibre-end cracks on E_L is incorporated into a calculation model where the fibre with its end cracks is decomposed into two kinds of inhomogeneities: a penny-shaped crack and a fibre of length $l - 2c$ with l and c being the length of a perfect fibre and the radius of the fibre-end crack, respectively. Thus, the whole composite contains three kinds of inhomogeneities: penny-shaped cracks, fibres of length l, and fibres of length $l - 2c$. By use of the above model and along with Eshelby's equivalent inclusion method and back stress analysis, Takao *et al.* [14] have computed E_L of completely aligned short fibre composite.

It should be noted that multiplying E_L for the aligned short-fibre composite with cracks by the orientation factor g_1 is a first-order approximation of $E_L^{(2)}$. It is also understood that the value of $E_L^{(2)}$ obtained by this procedure gives the secant modulus of the stress–strain curve since our model is based on a linear elastic analysis (with constant applied stress).

6. Results and discussion

Twenty per cent carbon short-fibre reinforced polyamide 66 [5] is used for the analytical study. Its material properties are given in Table I.

6.1. Computation of $E_L^{(1)}$

Curtis *et al* [5] made no measurement on the fibre orientation distribution and they deduced the fibre orientation factor from the rule-of-mixtures type formula. It should be noted that Fukuda and Chou [16] also adopted the step function type representation of fibre orientation distribution in the prediction of short-fibre composite strength. However, the transverse ($\sigma_0 \sin^2\theta$) and shear

TABLE I Material properties of 20% carbon short-fibre reinforced polyamide 66

Polyamide 66	$E_m = 2 \times 10^9$ Pa
	$\nu_m = 0.42$
	$\gamma_m = 300$ J [15]
Carbon fibre	$E_f = 2 \times 10^{11}$ Pa
	$\nu_f = 0.17$
	$l = 0.35$ mm
	$d = 0.007$ mm
Interface energy	$\gamma_I = 3.73$ J m^{-2}
Volume-fraction of fibre	$f_F = 0.2$

$(\sigma_0 \sin\theta\cos\theta)$ components were not taken into account.

Based on the work of Takao *et al.* [7], we have computed the longitudinal Young's modulus for the cases of aligned fibres ($\bar{E}_L$) and randomly oriented fibres with various values of α (E_L). The ratio $E_L/\bar{E}_L$ (defined by Equation 8) is plotted as a function of α in Fig. 5. For the data of Equation 17, we obtain $\bar{E}_L = 32.82$ GPa and the experimentally measured value of E_L is 24 GPa [5]. Thus, $E_L/\bar{E}_L = 0.73$, which yields the value of $\alpha = 31°$ from Fig. 5. Therefore, we predict that the orientation angle range α of the carbon short-fibre composite used by Curtis *et al.* [5] is about 31°.

6.2. Computation of σ_1

From Equations 11 and Table I, as well as $\alpha = 31°$ we obtain

$$\sigma_1 = 133 \text{ MPa}, \quad (17)$$

whereas the experimental value of σ_1 at $\epsilon = 0.0052$ is 124.8 MPa. Thus the value predicted theoretically is in good agreement with the experimental result.

6.3. Computation of σ_2

Before computing σ_2, we investigate the values of the critical stresses for the penny-shaped crack arrested by the adjacent fibres to penetrate through the fibre (σ_p) and for that to extend along the matrix–fibre interface (σ_I). According to [8], the above stresses for the present problem are:

$$\sigma_p = 160.47 \text{ MPa}$$
$$\sigma_I = 83.1 \text{ MPa} \quad (18)$$

In the derivation of Equation 18 we have used the average spacing between fibres of 0.02423 mm,

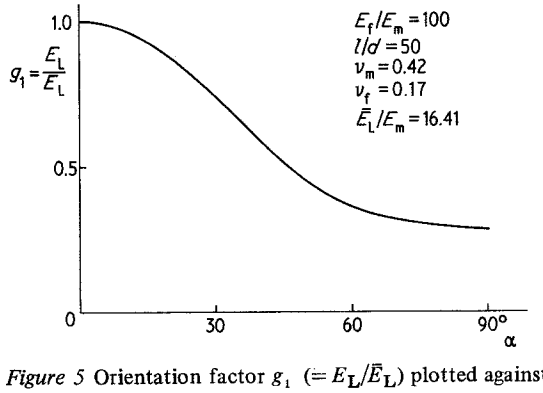

Figure 5 Orientation factor g_1 ($= E_L/\bar{E}_L$) plotted against the orientation range α.

which is based on the data of Table I and the model used in [5]. Now the critical stress for the penny-shaped crack (the solid curve in Fig. 4) to further extend into the matrix, σ_2, can be computed from Equation 13 as

$$\sigma_2 = 191.4 \text{ MPa}. \quad (19)$$

It follows from Equations 18 and 19 that the value of σ_2 exceeds those of σ_p and σ_I. Consequently, at applied stresses lower than the σ_2 the penny-shaped crack in Fig. 4 can advance from the position indicated by the dotted curve to that shown by the solid curve either by a debonding or penetration mechanism. There is no experimental data available for σ_2. However, we can use the fracture stress as σ_2 since the third stage of the composite deformation is very short and its value is estimated to be 210 MPa. Hence the theoretical value given by Equation 19 agrees well with the experimental value by neglecting the third stage of the stress–strain curve.

6.4. Computation of $E_L^{(2)}$

By using Equations 15 and 16 and Table I, taking α to be 31°, and the method by Takao *et al.* [14], we have computed $E_L^{(2)}$ at various applied stress levels σ, and the results are plotted in Fig. 6. It can be seen that $E_L^{(2)}$ reduces at a linear rate, which is in close agreement with the experiment as represented by Fig. 1b. The rate of slope change predicted theoretically is 1200 GPa which agrees reasonably well with the experimental result of 860 GPa.

6.5. Computation of the fracture strain ϵ_f

The fracture strain ϵ_f can also be computed by use of the value of σ_2 computed in Section 6.3 and that of the secant $E_L^{(2)}$ at $\sigma = \sigma_2$ obtained in Section 6.4. The value of ϵ_f predicted is 1.08% (Fig. 6), while the experimental value is 1.02%. Hence, the theoretical prediction is also in good agreement with the experiment.

7. Conclusions

(a) Theoretical analyses have been performed based upon the experimental observations that the short-fibre carbon/polyamide 66 systems deform in a highly elastic manner, and the non-linearity in the stress–strain curve is mainly due to the initiation and extension of fibre-end cracks. A typical stress–strain curve of this composite consists of three stages.

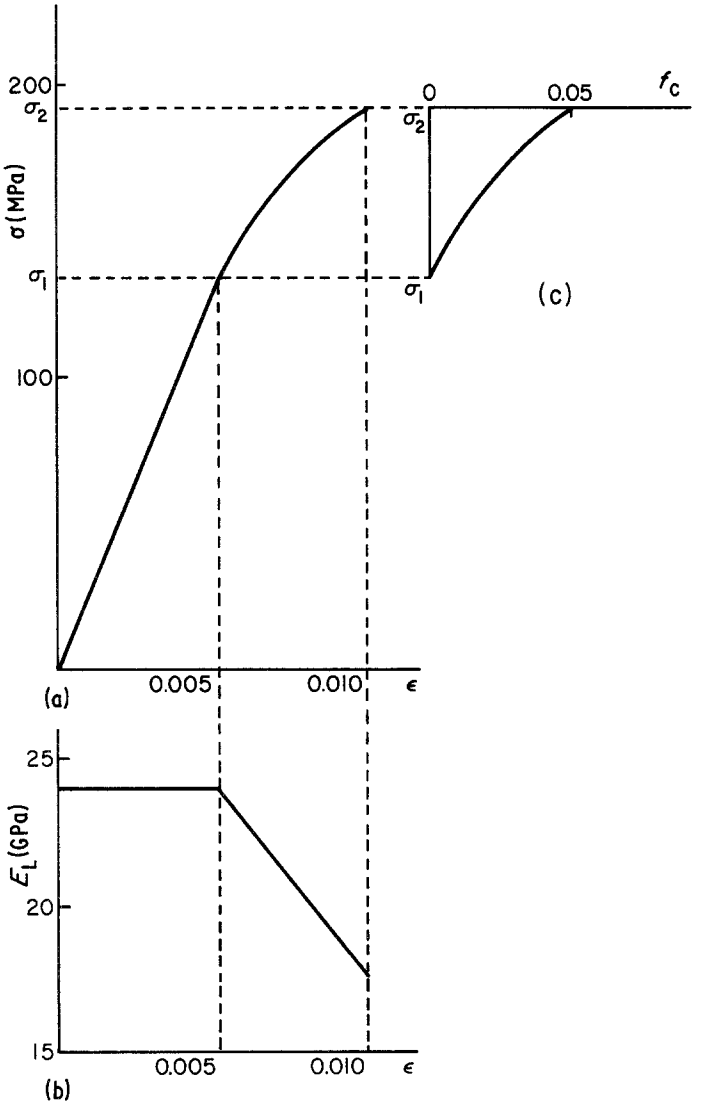

Figure 6 (a) Predicted stress–strain curve of misoriented 20% carbon short-fibre reinforced thermoplastic. (b) Tangent modulus, E_L, plotted against strain, ϵ. (c) The assumed crack density, f_c, as a function of applied stress.

(b) The first linear stage can be modelled by the elastic deformation of the composite system with misoriented short fibres. The second stage occurs due to the initiation of fibre-end cracks and their subsequent arrest by adjacent short fibres.

(c) The third stage deformation is modelled by the further extension of the arrested cracks in the matrix material.

(d) The analysis has taken into account the volume-fraction aspect ratio and orientation of the short fibres as well as the elastic properties and surface energies of fibre and matrix.

(e) Although the modelling of fibre orientation effect is a difficult task, it has been given consideration to the extent that the mathematical problems remain tractable.

(f) Close agreements between the theoretical predictions and experimental data have been obtained regarding the overall shape of the stress–strain curve, the transition stresses between two consecutive stages, and the failure strain of the composite.

Acknowledgements

This work is supported by the National Science Foundation (Grant No. CME-7918249). The authors also thank Y. Takao and H. Ishikawa for their help in some of the computations, and M. Bader for helpful discussions.

References

1. T. W. CHOU, S. NOMURA and M. TAYA, *J. Comp. Mater.* **14** (1980) 178.
2. S. NOMURA and T. W. CHOU, *ibid.* **14** (1980) 120.

3. *Idem, Int. J. Eng. Sci.* **19** (1981) 1.
4. H. FUKUDA and T. W. CHOU, *J. Mater. Sci.* **16** (1981) 1088.
5. P. T. CURTIS, M. G. BADER and J. E. BAILEY, *ibid.* **13** (1978) 377.
6. M. TAYA and T. W. CHOU, Proceedings of the Japan–US Conference on Composite Materials; Mechanics, Mechanical Properties and Fabrication, Tokyo, March, 1981, edited by K. Kawata and T. Akasaka (Japanese Society for Composite Materials), p. 119.
7. Y. TAKAO, T. W. CHOU and M. TAYA, Submitted.
8. H. ISHIKAWA, T. W. CHOU and M. TAYA, *J. Mater. Sci.* **17** (1982) 832.
9. J. D. ESHELBY, *Proc. Roy. Soc. (London)* **A241** (1957) 376.
10. M. TAYA and T. MURA, *J. Appl. Mech.* **48** (1981) 361.
11. M. TAYA and T. W. CHOU, *Int. J. Solids Structs* **17** (1981) 553.
12. T. MORI and K. TANAKA, *Acta Met.* **21** (1973) 571.
13. T. MURA, "Micromechanics of Defects in Solids" (Noordhoff, Eindhoven) (in press).
14. Y. TAKAO, M. TAYA and T. W. CHOU, *Int. J. Solids Structs.* in press.
15. A. PARVIZI, K. W. GARRETT and J. E. BAILEY, *J. Mater. Sci.* **13** (1978) 13.
16. H. FUKUDA and T. W. CHOU, *J. Mater. Sci.* **17** (1982) 1003.

Received 8 September 1981
and accepted 1 February 1982